Probing the Pore of ClC-0 by Substituted Cysteine Accessibility Method Using Methane Thiosulfonate Reagents

Chia-Wei Lin and Tsung-Yu Chen

Center for Neuroscience and Department of Neurology, University of California, Davis, CA 95616

ABSTRACT ClC channels are a family of protein molecules containing two ion-permeation pores. Although these transmembrane proteins are important for a variety of physiological functions, their molecular operations are only superficially understood. High-resolution X-ray crystallography techniques have recently revealed the structures of two bacterial ClC channels, but whether vertebrate ClC channel pores are similar to those of bacterial homologues is not clear. To study the pore architecture of the *Torpedo* ClC-0 channel, we employed the substituted-cysteine-accessibility method (SCAM) and used charged methane thiosulfonate (MTS) compounds to modify the introduced cysteine. Several conclusions were derived from this approach. First, the MTS modification pattern from Y512C to E526C in ClC-0, which corresponds to residues forming helix R in bacterial ClC channels, is indeed consistent with the suggested helical structure. Second, the ClC-0 pore is more accessible to the negatively charged than to the positively charged MTS compound, a pore property that is regulated by the intrinsic electrostatic potential in the pore. Finally, attempts to modify the introduced cysteine at positions intracellular to the selectivity filter did not result in larger MTS modification rates for the open-state channel, suggesting that the fast gate of ClC-0 cannot be located at a position intracellular to the Cl^- selectivity filter. Thus, the proposal that the glutamate side chain is the fast gate of the channel is applicable to ClC-0, revealing a structural and functional conservation of ClC channels between bacterial and vertebrate species.

KEY WORDS: MTS modification • SCAM • charge selection • state dependence

INTRODUCTION

The ClC channel family comprises members widely distributed in different living species from bacteria to vertebrate animals (Jentsch et al., 1999, 2002; Maduke et al. 2000; Hille, 2001). These channels are unique in that two identical ion-conducting pores are present in a channel molecule. Recently solved high-resolution X-ray structures of the bacterial ClC channels have provided a basis for understanding the molecular operations of these anion channels (Dutzler et al., 2002, 2003). The structures show that ClC channels are homodimers containing two pores, and each pore is formed entirely by a subunit containing 18 α-helices named helix A to R. These helices wrap around a common center, and the amino acids at the NH_2-terminal end of the α-helices are brought together to coordinate the bound chloride (Cl^-) ion at a site (the central site, S_{cen}) likely to serve as the ion selectivity filter (Dutzler et al., 2002). Besides the S_{cen} site, there are two other Cl^- binding sites found in the ion permeation pathway: one internal to the S_{cen} site, and the other located external to S_{cen} at a position of the negative charge on a glutamate residue (Dutzler et al., 2003). This glutamate residue, which corresponds to glutamate 166 (E166) of ClC-0, projects its negatively charged side chain into the ion permeation pathway to occlude the ion flux. Competition of Cl^- with this glutamate side chain has been proposed to be responsible for the coupling of gating to the ion permeation (Dutzler et al., 2002, 2003). Although not as clear as the pore in the KcsA K^+ channel (Doyle et al., 1998), the bacterial ClC channel structures also suggest the Cl^- permeation pathway. In particular, basic amino acid residues in the internal and external pore entrances were thought to be important in funneling the permeant ions to the pore (Dutzler et al., 2002).

Although these interesting structural features in the bacterial ClC channels are very informative, the difficulty in recording the bacterial ClC channels with conventional electrophysiological techniques has impeded the studies of the structure-function relation in bacterial ClC channels. ClC-0 from the electric organ of *Torpedo* rays (Jentsch et al., 1990; O'Neill et al., 1991) provides a model system to understand the channel functions. Significant characterization of ClC-0 properties has been obtained from functional recordings of this

Chia-Wei Lin's present address is Center for Research on Occupational and Environmental Toxicology, Oregon Health and Science University, Portland, OR 97201.

Address correspondence to Tsung-Yu Chen, Center for Neuroscience, University of California-Davis, 1544 Newton, Court Davis, CA 95616. Fax: (530) 754-5036; email: tycchen@ucdavis.edu

**Abbreviations used in this paper:* HEK, human embryonic kidney; MTS, methane thiosulfonate; SCAM, substituted cysteine–accessibility method; WT, wild-type.

J. Gen. Physiol. © The Rockefeller University Press • 0022-1295/2003/08/147/13 $8.00
Volume 122 August 2003 147–159
http://www.jgp.org/cgi/doi/10.1085/jgp.200308845

Torpedo channel in the past two decades. For example, the "double barrel" feature of the channel was predicted based on the binomial distribution of the three current levels found in single-channel recording traces of ClC-0 (Miller, 1982; Hanke and Miller, 1983; Miller and White, 1984; Middleton et al., 1994, 1996; Ludewig et al., 1996; Lin and Chen, 2000). The proposal that the permeant ion may compete with the negatively charged side chain of the glutamate to open the pore is used to explain the previous functional observation that the gating of ClC-0 is tightly coupled to ion permeation (Pusch et al., 1995; Chen and Miller, 1996). Finally, a positively charged lysine residue at the inner pore mouth of ClC-0 has been demonstrated to control the pore conductance (Middleton et al., 1996; Chen and Chen, 2003). These channel properties derived from functional studies of ClC-0 appear to fit the structures of the bacterial ClC channels quite nicely.

Although the above properties of ClC-0 appear to find support from the bacterial ClC channel structures, other aspects of the channel remain uncertain. First, the *Torpedo* ClC-0 channel is known to have two distinct gating mechanisms, a fast and a slow (inactivation) gating, each operating at very different time scales (for review see Miller and Richard, 1990; Maduke et al., 2000). The crystal structures of bacterial ClC channels, however, have suggested only one gate, the side-chain of a glutamate residue. One might be curious which gating mechanism, the fast or the slow gating of ClC-0, corresponds to the glutamate gate observed in bacterial ClC channel structures. Even though bacterial ClC channel structures show a glutamate side chain in each pore, suggesting that this side chain is more likely to be the fast gate, the absence of the structure for the COOH-terminal half of the ClC-0 molecule makes this assertion less certain. Second, the bacterial ClC channel structures provide a structural basis for identifying the pore-lining residues in the ion-permeation pathways. In comparison with the structure of KcsA K^+ channel, however, the two ion permeation pathways in bacterial ClC channels are more obscure. For example, the bound Cl^- ions at the selectivity filter are nearly invisible from the pore entrances. The curved ion permeation pathway, as defined by the bound ions and the crucial charged residues in the pore (Dutzler et al., 2002, 2003), is void of water filled space as the one observed in the KcsA K^+ channel (Doyle et al., 1998). Therefore, whether the 20% sequence-identity *Torpedo* homologue adopts a similar pore structure is unknown. A direct exploration of the ClC-0 pore will thus complement bacterial ClC channel structures to define the pore residues of the ClC-0 channel.

To understand if the pore architecture is conserved between ClC-0 and bacterial ClC channels, we employed substituted cysteine–accessibility method (SCAM)* and used methane thiosulfonate (MTS) reagents to probe the putative inner pore region of ClC-0. SCAM has been widely employed in a variety of cation and anion channels (Akabas et al., 1992; Lu and Miller, 1995; Cheung and Akabas, 1997; Fahlke et al., 1997; Liu et al., 1997; Karlin and Akabas, 1998; Lu et al., 1999; Reeves et al., 2001). By comparing the reaction rates of the negatively and positively charged MTS reagents with the cysteine in the pore, it is possible to measure the extent of anion to cation selectivity in the pore (Cheung and Akabas, 1997; Pascual and Karlin, 1998; Wilson et al., 2000). Studying the accessibility of the introduced cysteine to MTS reagents at open and closed states would also reveal potential state-dependent modifications, which may be used to argue for the presence of a gate (Liu et al., 1997). In the present study, we introduce cysteine at the positions from Y512 to E526 (see also Ludewig et al., 1997), residues that potentially form an α helix (helix R, according to the bacterial ClC structures) extending from the S_{cen} site to the proposed inner pore mouth. We also place a cysteine in place of S123. The side chain of the corresponding serine of the bacterial ClC channel coordinates the bound Cl^- at S_{cen}. Comparisons of the modification rates of MTS reagents with the introduced cysteine at these positions reveal that a more positive intrinsic electrostatic potential is encountered by the MTS reagents as the introduced cysteine is located deeper in the pore. Altering the side-chain charge of the amino acid residues in the pore also significantly changes the MTS modification rate, suggesting that the charges of the pore residues participate in selecting anionic over cationic MTS reagents. We have also conducted experiments to examine if there is a state-dependent modification by MTS reagents of a cysteine placed at various positions in the pore.

MATERIALS AND METHODS

Mutagenesis, Channel Expression, and Transfection

Site-directed mutagenesis was performed using PCR-based techniques, and the mutations were confirmed by DNA sequencing. All the cysteine mutants in the present study are created in the background of the C212S mutation (Lin et al., 1999), and therefore this inactivation-suppressed mutant will be referred to as the wild-type (WT) channel. For channel expressions in *Xenopus* oocyte, all the mutants were constructed in the pBluescript vector (Stratagene). The method for RNA synthesis and the injection of RNA into oocytes have been described in previous studies (Chen, 1998; Lin et al., 1999; Lin and Chen, 2000; Chen and Chen, 2003). For channel expression in human embryonic kidney (HEK) 293 cells, mutant plasmids in pBluescript vector were digested with two restriction enzymes, KpnI and AgeI (New England Biolabs, Inc.). The cDNA fragments containing the mutations were sub-cloned into a WT ClC-0 constructed in the pcDNA3 vector.

HEK 293 cells were plated into a 35-mm culture dish (Corning, Inc.) at a density of 3×10^5 per well one day before transfec-

tion. The medium was the antibiotics-free Dulbecco's Modified Eagle Medium supplemented with 20 mM L-glutamine and 10% fetal bovine serum. Upon transfection, cells usually grew to >90% confluence, and 1–3 μg of the channel cDNA and 0.4–0.7 μg of green fluorescence protein (GFP) cDNA were cotransfected into the cells with Lipofectamine™ 2000 (GIBCO BRL) according to the procedures from the manufacturer. On the day when the recordings were performed (usually 24–48 h after transfection) the cells were dissociated into individual cells with 1 × EDTA/Trypsin (GIBCO BRL) and plated onto coverslips coated with 0.01% poly-L-lysine (Sigma Aldrich). The cells were allowed to settle down onto the coverslip for two hours, and identification of the transfected cells was facilitated through GFP protein using a fluorescence microscope (Leica DM IRB).

Electrophysiological Recordings

The excised inside-out patch configuration (Hamill et al., 1981) was used throughout all recordings. Borosilicate glass electrodes were pulled by PP-830 puller (Narashige Co.), and when filled with the pipette solution, have resistance of ~1–2 MΩ. For recordings of HEK 293 cells, the standard bath (intracellular) solution consisted of (in mM): 130 NaCl, 5 HEPES, 5 $MgCl_2$, 1 EGTA, pH = 7.4. The pipette (extracellular) solution contained (in mM): 130 NMDG-Cl, 5 HEPES, 5 $MgCl_2$, 1 $CaCl_2$, pH = 7.4. In the experiments using an extracellular solution containing only 4 mM Cl^-, the 130 mM NMDG-Cl in the pipette solution was replaced with 130 mM NMDG-glutamate and 5 mM $MgCl_2$ was changed to 1 mM. For single-channel recordings, the bath and the pipette solutions were described previously (Lin and Chen, 2000; Chen and Chen, 2003). The pH of the bath and the pipette solution was titrated with NaOH and NMDG, respectively.

Macroscopic currents recorded from HEK 293 cells were low-pass filtered at 1kHz (digital filter associated with the acquisition software) and were digitized by Digidata 1320 acquisition board (Axon Instruments, Inc.) at 5 kHz with pClamp8 software. Out of the 16 mutants, only L521C did not produce large enough current for functional studies. To evaluate the mutation effects of introducing a cysteine residue to various positions, a series of voltage steps was delivered to the membrane patch to elicit a family of macroscopic currents that allows a calculation of the P_o of the channel. Examples from the WT channel and several cysteine mutants are displayed in Fig. 1. Such a voltage protocol contains a prepulse voltage step to 60 or 80 mV for 100 ms, followed by different test voltages from 100 or 80 mV to −160 mV in −20-mV steps for 200 ms. The tail current was measured with a voltage step to −100 mV for 150 ms. The steady-state P_o for all the channels except S123C (see text in RESULTS) was estimated by normalizing the initial tail current to the one following the most depolarized test pulse (100 or 80 mV).

MTS Modification

MTSES (2-sulfonatoethyl MTS) and MTSET (2-(trimethylammonium)ethyl MTS) were purchased from Toronto Research Chemicals and were prepared as 100- or 300-mM stock solutions in ddH_2O stored at −80°C. Upon use, an aliquot of the stock solution was thawed into the working solution right before the application of the reagents. Solution exchange was achieved using SF-77 solution exchanger (Warner Instruments). The modification procedures are as follows. The holding potential of the inside-out patch was at 0 mV, and the voltage protocol used in the modification experiments contains a modification voltage (V_{MO}) step followed by a monitoring voltage (V_{MN}) step. The duration of V_{MO} was 550 or 950 ms, and this voltage step was divided into three sections. The first section of 100 ms allows the gating relaxation reach to a steady-state in control solution. In the second section, a digital signal from Digidata 1320 board was used to move the solution-delivering pipes so that the patch was exposed for 400 or 800 ms to the solution containing MTS reagents. The delay in the solution exchange was ~30–35 ms as judged from a separate junction potential measurement. Thus, the final 50-ms section at V_{MO} allowed the patch to fully return to the control solution before the voltage was step to V_{MN}. In experiments at high external Cl^- concentration ($[Cl^-]_o$) V_{MN} was usually at 60 or 80 mV, and the current was measured at the steady-state. However, the modifications of K519C and I515C/K519E with MTSET were monitored at −40 mV because the current increases much more at the negative potential than at the positive potential. In experiments using 4 mM Cl^-, the current was monitored by a voltage step to 80 mV followed by a 0-mV voltage step. The initial current at 0 mV reflects the amount of the current flowing through the fully open channels at the preceding voltage step of 80 mV. These measured currents were plotted against the accumulative MTS exposure time, or the accumulative MTS exposure (concentration × time) in Figs. 8 C and 9 A.

Single-channel Recordings

To compare the MTS modification effects of the cysteine mutants between macroscopic and single-channel current levels, MTS modifications at single-channel level were also performed in some of the mutants expressed in *Xenopus* oocytes (see Fig. 3). Detailed procedures of single-channel recordings and analyses were described in the previous papers (Lin et al., 1999; Lin and Chen, 2000; Chen and Chen, 2001, 2003).

Data Analysis

Except where indicated, all MTS modification processes were fitted to a single-exponential equation,

$$I_t = I_\infty + (I_0 - I_\infty)\exp(-t/\tau),$$

where I_t is the measured current at the accumulative exposure time t, I_0 is the initial current, I_∞ is the current when the modification is reached to a steady-state, and τ is the time constant of the modification process. The curve fitting was performed with an unweighted least-squares method using Clampfit 8 software (Axon Instruments, Inc.). The time constant τ and the concentration of MTS reagents were used to calculate the second order rate constant k according to the following equation:

$$k_{MTS} = 1/(\tau[MTS]).$$

All data points in this study were the average of at least three independent measurements, and the numbers are presented as mean ± SEM.

RESULTS

Mutating the amino acid to cysteine sequentially from residue 512 to 526 of ClC-0 that align to helix R of the bacterial ClC channel gave rise to functional mutants in most of the cases. Except K519C and S123C, most of these cysteine mutants have a similar pattern in the macroscopic current as that of the WT channel (Fig. 1). For the K519C mutant, the slight outward rectification of the instantaneous current is likely due to the rectification of the single-channel current (Middleton et al., 1996), whereas the slower current deactivation is

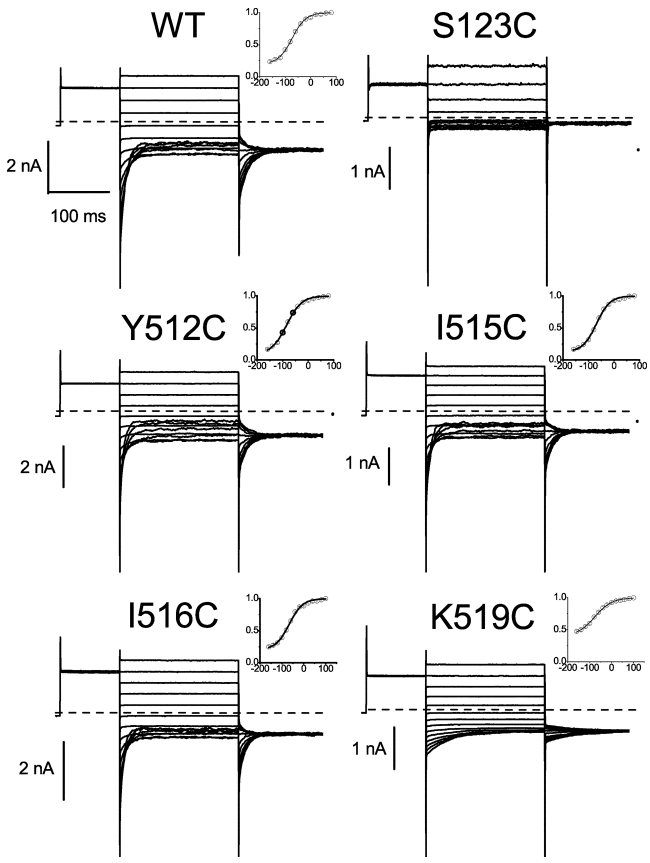

FIGURE 1. Effects of cysteine mutations at various positions in ClC-0. All recordings were from excised inside-out patches. Insets are fast-gate P_o-V curves derived from normalization of the initial tail current following each individual test voltage (see MATERIALS AND METHODS for the detailed voltage protocol).

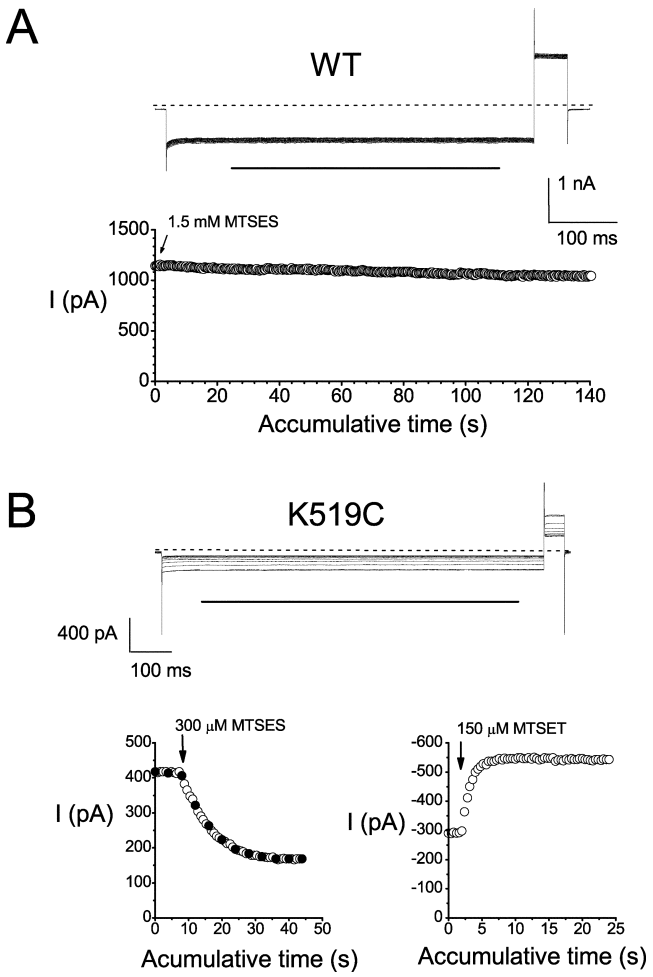

FIGURE 2. Voltage protocol used to modify the introduced cysteine at a desired voltage. (A) Modification of the WT channel with MTSES. Top panel shows the original recording traces (only one out of 10 traces shown). Modification voltage (V_{MO}) was −40 mV, while the modification time was 400 ms (straight line). The current was measured at the end of the monitoring voltage (V_{MN}) of 60 mV. The pulse was repeated once every 2 s, and the measured current was plotted against the accumulative MTSES exposure time. Note that even with 1.5 mM MTSES, the modification of the WT channel was insignificant. (B) Modification of the K519C mutant with MTSES and MTSET. Top panel shows one out of five original traces for 300 μM MTSES modification represented by the solid circles shown in the bottom left panel. The exposure time to MTS reagent in each pulse was 800 ms (straight line) in this experiment. V_{MO} was −40 mV and V_{MN} was 60 and −40 mV for MTSES and MTSET, respectively. Note that for the plot of MTSET modification (bottom right), the y-axis is in opposite direction as that in the MTSES plot (bottom left).

due to a reduction in the fast-gate closing rate. However, the fast-gate P_o of this mutant, like that of the WT channel, is close to unity at the most depolarized potential, allowing the construction of the steady-state P_o-V curve. The only mutant that prevents the evaluation of the fast-gate P_o from macroscopic current is S123C. The P_o of this mutant does not reach to unity even at 80 mV, as judged from the prominent noise from the recording trace (also see Fig. 8 A). Direct observations of the channel behaviors at the single-channel level also indicate that the fast-gate closing rate of S123C is very fast (see below), resulting in a very fast macroscopic current deactivation that cannot be easily separated from the capacitance current.

Modifications of the WT and the cysteine mutants with MTS compounds have different functional consequences depending on the positions of the introduced cysteine and the charge of the modifying reagent. Even though there are 11 native cysteine residues in the WT channel (C212 has been removed in the "WT" channel referred in this study), applications of MTSES or MTSET to the intracellular side of the WT channel have little effect in altering the current (Fig. 2 A). On the other hand, MTSES decreases and MTSET increases the current of the K519C mutant (Fig. 2 B); the results directly reflect the modification effects on the single-channel conductance of this mutant (Middleton et al., 1996; Chen and Chen, 2003). For the other cysteine

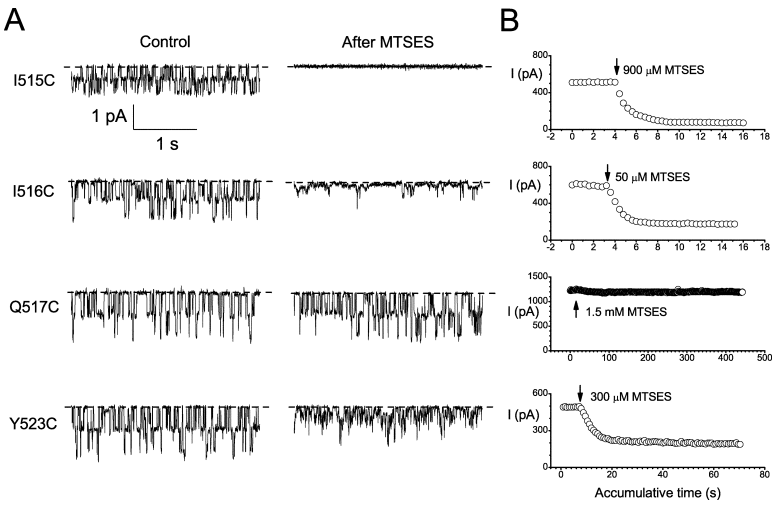

FIGURE 3. Functional consequences of MTSES modifications of various cysteine mutants. (A) Modification effects at the single-channel level. Recordings were from excised inside-out patches from *Xenopus* oocytes. External and internal Cl^- concentrations were both 120 mM. Recording voltages were −60 mV for I515C, and were −90 mV for the other three mutants. (B) MTSES modifications at the macroscopic current level. Recordings were from excised inside-out patches from HEK 293 cells. V_{MO} = −40 mV. Note that the residual currents were correlated well with those observed at the single-channel level shown in A.

mutants, MTS modifications can completely inhibit the current, partially alter the current, or have very little effect on the current (Fig. 3).

The overall results of MTSES and MTSET modifications of the 16 mutants examined in this study are shown in Fig. 4 A. 1 out of these 16 mutants, L521C, as indicated by the symbol "#" in Fig. 4 A, did not generate a large enough current for macroscopic current recordings (three runs of expression attempts). 2 out of those 15 functional mutants (K520C and E526C, indicated by the symbol "+" in Fig. 4 A) did not show an alteration of the current upon high concentrations (up to 1.5 mM) of MTSES and MTSET applications. At the present time, we could not differentiate if the absence of MTS modification effect in these two mutants is due to a lack of modification or because of no functional consequence after cysteine modification. For the rest of the mutants, both MTSES and MTSET can modify the introduced cysteine. In Q517C and I518C mutants, MTSET modification inhibits the current, while MTSES modification has little effect in altering the current. However, MTSES did modify both mutants because if the patch was first exposed to MTSES, subsequent MTSET modification was abolished (unpublished data). By the same argument, MTSET can modify P525C, but the modification has little functional effect. MTS modification rates in these three mutants (indicated by the symbol "★" in Fig. 4 A) therefore can be precisely measured only from one MTS reagent.

For the 13 cysteine mutants whose currents are susceptible to MTSES and/or MTSET modifications, the second order modification rate constants (V_{MO} = −40 mV) are compared in Fig. 4 A. The modification rates of these mutants may seem to have no particular interesting pattern at a first glance. However, a careful comparison reveals that four positions stand out and show faster modifications than the rest of the mutants, P522C, K519C, I516C, and D513C. In every third position along the sequence, the MTS reagents give a faster modification rate. This might suggest that these four positions are more exposed to the aqueous solution. For the other positions, however, the introduced cysteine still reacts with both MTSES and MTSET significantly. Even for the two mutants S123C and Y512C, the modification rates at −40 mV for MTSES and MTSET are ∼200–600 $M^{-1}s^{-1}$. Because these two residues are at the deepest locations in the pore, the other truly exposed pore residues should be more accessible to MTS reagents than these two residues. Thus, we set a criterion for picking up the exposed residues: their MTSES and MTSET modification rates are both larger than those of S123C and Y512C. Applying this criterion eliminates L524C and S514C from the 10 mutants that are functionally susceptible to both MTSES and MTSET modifications. In Fig. 4 B, the positions of the more exposed positions are shown in red, whereas the other positions in helix R are in yellow. It is interesting to observe that the "hot" spots are all positioned on one side of the suggested R helix, and this more exposed side appears to face the two permeant ions (see Fig. 4 B). Thus, this modification pattern is consistent with the idea that residues 512–526 of ClC-0 indeed form a helix, and suggests that these exposed residues likely line the wall of the pore.

The comparison of MTSES and MTSET modification rates in these more exposed residues reveals another interesting observation: they are quite similar to each other for most of the mutants even though MTSET is known to have a higher intrinsic reactivity with the free thiol in the bulk solution (Stauffer and Karlin, 1994). To examine this issue more closely, we calculate the ratio of the modification rates between MTSES (k_{MTSES}) and MTSET (k_{MTSET}) for those residues that are likely

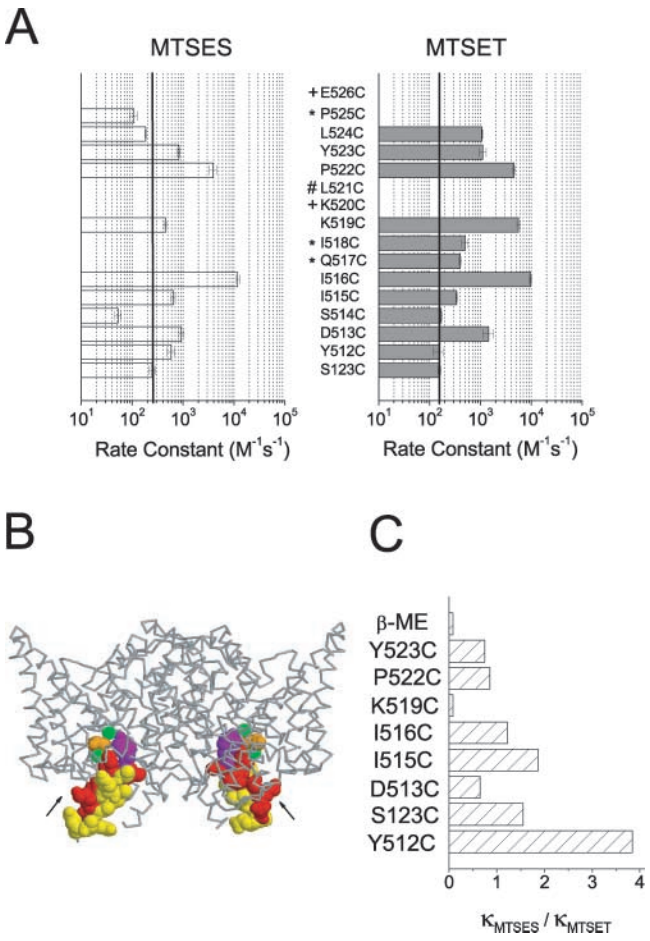

FIGURE 4. Comparison of the MTSES and MTSET modification rates for the cysteine mutants. (A) Second order rate constants of MTSES and MTSET modifications for various mutants. V_{MO} = −40 mV. For the meanings of the symbols labeled on the left of the mutants, see text in RESULTS. The vertical solid line in each panel represents the smaller value of either S123C or Y512C. (B) The positions with higher modification rates line up on one side of the R helix. *E. coli* ClC channel structure was taken from the Protein Data Bank (code 1OTS) with the cocrystallized antibody molecules removed. Green spheres represent Cl^- ions. S107 (S123 of ClC-0) and Y445 (Y512 of ClC-0) are in orange and purple, respectively. Arrows depict the intracellular pore entrances. The positions with larger MTSES and MTSET modification rates than those indicated by the vertical lines in A are shown in red. All the other residues in helix R are shown in yellow. (C) Comparison of the MTSES and MTSET modification rates by taking the ratio of the MTSES and MTSET modification rates. Only those mutants whose MTSES and MTSET modifications were both faster than the values indicated by the solid lines in A (the red positions in B) are compared.

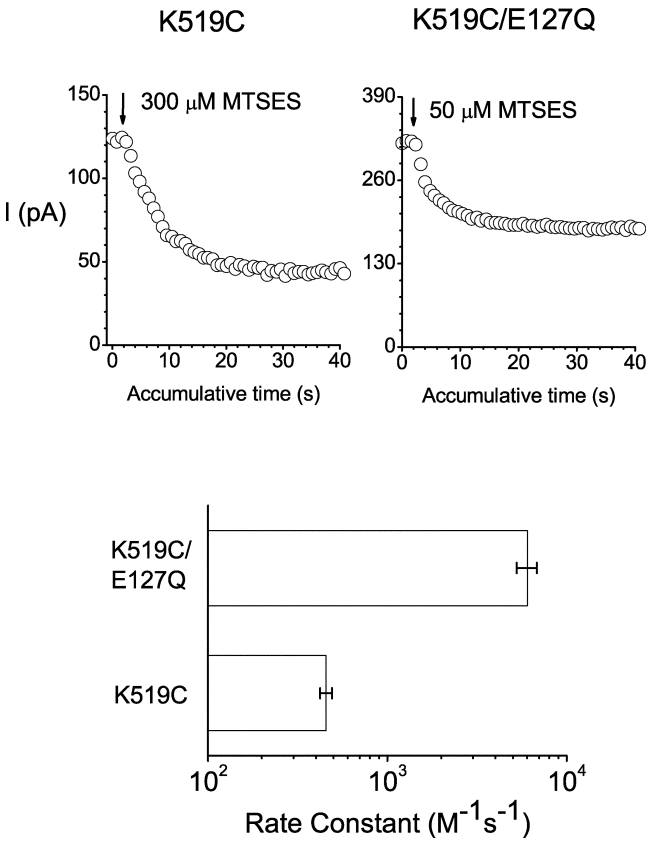

FIGURE 5. Side-chain charge effect from E127 on the MTSES modification rate of the cysteine introduced at position 519. V_{MO} = −40 mV and V_{MN} = +60 mV. By removing the negative charge at the E127 position, the MTSES modification rate is increased by 14-fold. At the same time, the residual current after MTSES modification is increased, reflecting the effect of E127Q mutation on the single-channel conductance of the channel in which residue 519 is negatively charged (see Chen and Chen, 2003).

exposed to the aqueous solution. This ratio reflects the charge selection at the position where the introduced cysteine is placed, and may be used to imply the anion to cation (or vice versa) selectivity of the pore (Cheung and Akabas, 1997; Pascual and Karlin, 1998; Wilson et al., 2000). Fig. 4 C plots the ratios of k_{MTSES}/k_{MTSET} for the six mutants shown in red in Fig. 4 B, those for the mutants S123C and Y512C, and the ratio of modifying β-mercaptoethanol (β-ME) taken from the study of Stauffer and Karlin (1994). It is interesting to observe that as the position is deeper in the pore, the ratio k_{MTSES}/k_{MTSET} generally becomes larger, with two exceptions: K519C and D513C—both mutations convert a charged amino acid to a cysteine. The deviation from the general trend of increasing the ratio at positions 519 and 513 was therefore ascribed to the alteration in the intrinsic electrostatic potential of the pore due to the neutralization of charged residue by the mutation. Because the inner pore residues of ClC-0 control the conductance of ClC-0 (and thus the Cl^- flux) electrostatically (see Chen and Chen, 2003), we suspected that the same electrostatic regulations also contribute to the selection of the charged MTS reagents. To examine this possibility, we made a double mutant E127Q/K519C, and compared its MTS modification rates with those of the K519C mutant. At the same membrane potential, removing the negative charge at position 127 increases

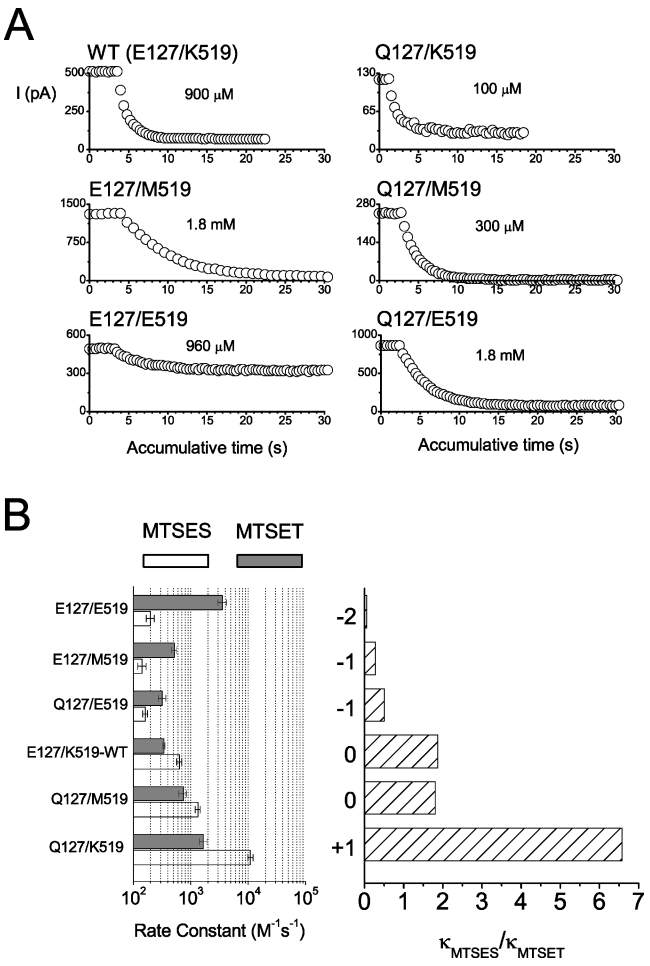

FIGURE 6. Electrostatic control of the MTS modification rates by charged residues at the inner pore mouth. (A) MTSES modifications of various charge combination mutants. (B) Comparison of the second order rate constants of MTSES and MTSET modifications in various charge combination mutants.

the MTSES modification by ~14-fold (Fig. 5). Unfortunately, in the presence of E127Q mutation, modifying the cysteine at position 519 with MTSET did not have an effect on the macroscopic current (unpublished data). This is because in the E127Q background, the channels with a positive and a neutral charge at position 519 have similar conductance (see Chen and Chen, 2003). Without a prominent modification effect, the MTSET modification rate cannot be precisely determined in the E127Q/K519C double mutant.

To circumvent this problem, we introduce cysteine at position 515 and alter the charge at positions 127 and/or 519. Fig. 6 A shows the experiment for MTSES modification of I515C in various background charge combinations for positions 127 and 519. The second order rate constants for MTSES and MTSET modifications and the ratios of k_{MTSES}/k_{MTSET} for these mutants are plotted in Fig. 6 B. It can be seen clearly that as the overall charge from positions 127 and 519 is made more negative, the MTSES modification rate is reduced while the MTSET modification rate is increased. When these positions are made more positive, the MTSES modification rate increases as expected, but the MTSET modification rate is paradoxically increased. However, the ratio of k_{MTSES}/k_{MTSET} increases monotonically by >110-fold when comparing the one in Q127/K519 channel with that in the E127/E519 channel. Like the regulation of the single-channel conductance, position 127 has a stronger effect in altering the absolute value of MTS modification rate. For example, removing one positive charge at position 519 (Q127/K519 versus Q127/M519) reduces the MTSES modification rate by ~10-fold, while adding a negative charge onto position 127 (Q127/K519 versus E127/K519) reduces the MTSES modification rate by >20-fold. However, in terms of k_{MTSES}/k_{MTSET} ratio, altering the charge at position 127 is roughly equivalent to changing the charge at position 519.

Thus, the above results suggest that the pore architecture of ClC-0 appears to be similar to those seen in the bacterial ClC channels—the modification pattern from Y512C to E526C is consistent with a helical structure, and the charges at these positions also help select anions over cations. Therefore, helix R of ClC-0 is likely to line the wall of the pore. Because mutations at the inner pore mouth change the fast gating property of the channel (for example, K519E mutation, see Pusch et al., 1995; Chen and Chen, 2003), we ask if there is a physical gate internal to the S_{cen} site. Modifications of the introduced cysteine have been used to suggest the presence of a physical gate if the introduced cysteine reacts with MTS reagents significantly faster when the channel is open than when the pore is closed (Liu et al., 1997). At more superficial positions, positions 523 and 519, no significant difference in the MTSES modification rate was observed between conditions in which the P_o of the fast gate are <0.25 and >0.97 (unpublished data). In another experiment, the cysteine at a deeper position, I515C, was examined (Fig. 7). In this mutant, two approaches were used to dissect out the state dependence from the voltage dependence of MTS modifications. First, we took advantage of the fact that the fast-gate P_o is significantly changed by varying $[Cl^-]_o$ (Fig. 7 A), and compared the MTSES modification rate at the same voltage but at different $[Cl^-]_o$ (Fig. 7 B). Second, we studied MTSES and MTSET modifications at different voltages (Fig. 7, C and D). In both approaches, the modification rates for MTSES and MTSET in various conditions were ~300–700 $M^{-1}s^{-1}$, and we did not observe a consistent increase of MTS modification rate when the P_o of the fast gate is increased. In contrast, the MTSES modification rate appears to decrease as the P_o of the fast gate increases

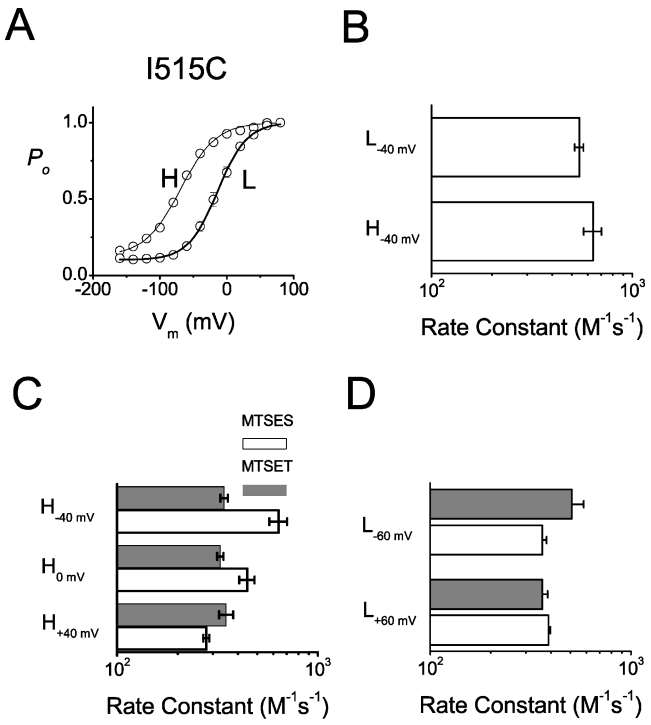

FIGURE 7. Examination of state-dependent modification for the I515C mutant. (A) Steady-state P_o-V curves of the I515C mutant at a high (H, 142 mM) and a low (L, 4 mM) $[Cl^-]_o$. (B) Comparison of the MTSES modification rate at the same voltage, but at different $[Cl^-]_o$. The P_o for the conditions of $L_{-40\ mV}$ and $H_{-40\ mV}$ were 0.32 and 0.79, respectively, as shown from the P_o-V curve plot in A. The difference between the modification rates of these two conditions is not statistically significant ($P > 0.05$, Student's t test). (C) Comparison of the second order rate constants for MTSES and MTSET modifications in the high $[Cl^-]_o$ condition at three different voltages. The three MTSET modification rates do not show statistically significant differences, while the MTSES modification rate at $H_{+40\ mV}$ is significantly different from the other two MTSES modification rates. (D) Comparison of the modification rate at the same low $[Cl^-]_o$, but at two different voltages. The P_os under these two conditions were 0.19 ($L_{-60\ mV}$) and 0.97 ($L_{+60\ mV}$), respectively. The modification rates between the two conditions are not statistically different for both MTSES and MTSET modifications.

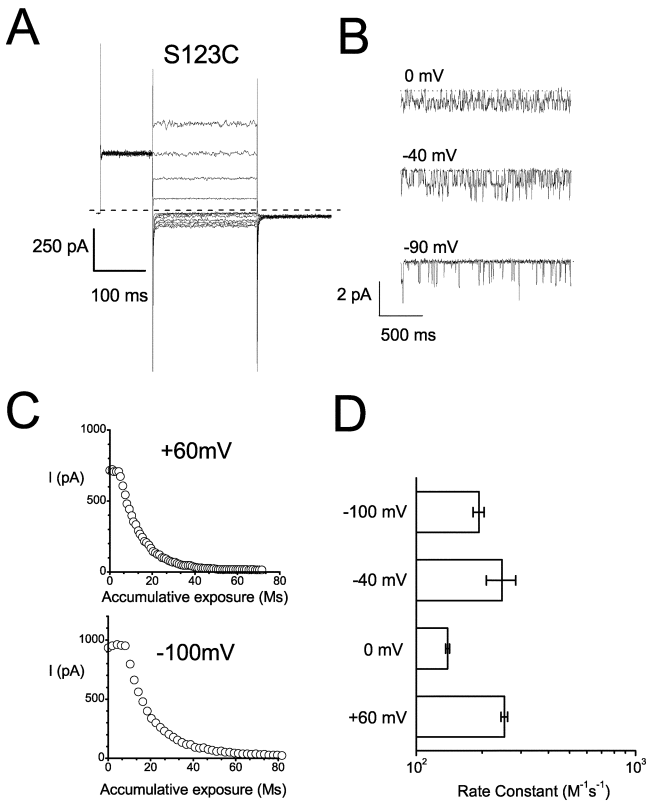

FIGURE 8. MTS modifications for the S123C mutant. (A) Macroscopic current from S123C mutant before MTSES modification. (B) Single-channel recordings of the S123C before MTS modifications. External and internal Cl^- concentrations were 120 and 2,400 mM, respectively. (C) MTSES modifications of the S123C mutant at two voltages with significant difference in P_o. (D) Comparison of MTSES modification rates of S123C at four different voltages. Only the modification rate at 0 mV is significantly different from the other conditions.

(Fig. 7 C). These experiments suggest that the fast gate cannot be on the intracellular side of the position 515 in ClC-0.

The voltage-dependent change of the fast-gate P_o is most prominent in the mutant S123C. Fig. 8 A shows the macroscopic current, and Fig. 8 B shows the single-channel recording traces of this cysteine mutant. Because the closing rate of the channel is very fast, we use an internal Cl^- concentration of 2,400 mM to slow down the closing rate of the channel in single-channel recording experiments (Chen and Miller, 1996). However, even under such a high internal Cl^- concentration, the P_o of the channel is small at negative voltages. In the presence of physiological Cl^- concentrations on both sides of the membrane, the closing rate of the channel is so fast that the deactivation of the macroscopic current cannot be easily separated from that of the capacitance current. Even at a voltage of 80 mV (the most depolarized voltage in Fig. 8 A), the large noise from the recording trace suggests that the fast-gate P_o is not close to unity. Therefore, the severe outward rectification in the macroscopic current recording is most likely due to a significant increase of P_o when the voltage is depolarized. We therefore compare the MTSES modification rates at four voltages (Fig. 8, C and D). Again, the modifications do not show a consistent pattern of higher modification rate when the P_o of the channel is raised.

Finally, we studied the modification of the cysteine introduced at another position at S_{cen}, Y512. Fig. 9 A shows the comparison of MTSES and MTSET modifications at two voltages where the values of fast-gate P_o are very different. It can be clearly seen that when the fast-gate P_o is raised from −80 to +60 mV, the MTSES modification rate is significantly reduced while the MTSET

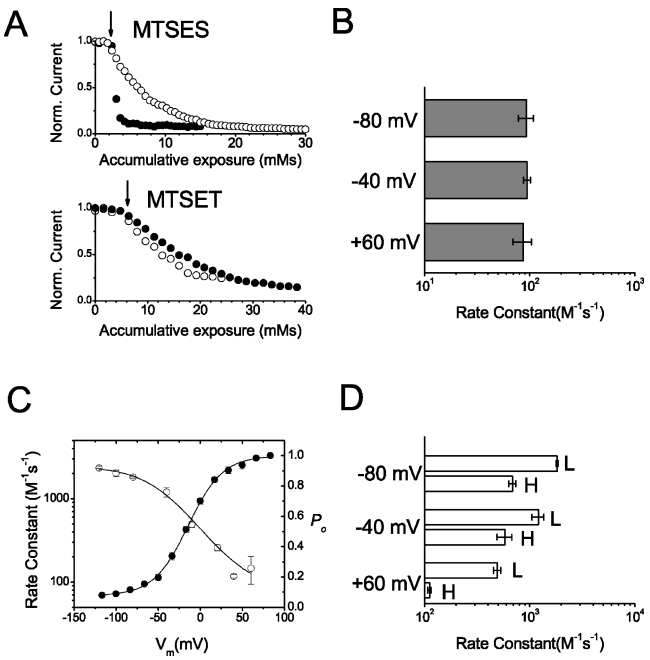

FIGURE 9. MTS modifications for the Y512C mutant. (A) Comparison of MTSES and MTSET modification rates at −80 mV (filled symbols) and +60 mV (open symbols). $[Cl^-]_o$ was 4 mM to shift the fast-gate P_o-V curve to a technically convenient position so that the P_o at these two voltages significantly differs from each other. The horizontal axis represents the concentration (mM) × cumulative exposure time (s). (B) Second order rate constants of MTSET modification at three voltages. $[Cl^-]_o$ = 4 mM. The P_os at these three voltages are: 0.20 (−80 mV), 0.51 (−40 mV), and 0.98 (+60 mV). (C). Steady-state P_o-V curves (filled symbols) and the MTSES modification rates (open symbols) at 4 mM external Cl^-. Solid curves are drawn according to Boltzmann equations. (D) Comparison of the MTSES modification rates from the same voltage at different $[Cl^-]_o$. L: $[Cl^-]_o$ = 4 mM. H: $[Cl^-]_o$ = 142 mM. The P_os at high $[Cl^-]_o$ are: 0.60 (−80 mV), 0.84 (−40 mV), and 0.99 (+60 mV). At all three voltages, the differences between low (L) and high (H) $[Cl^-]_o$ are statistically significant. Note that at +60 mV, the difference in MTSES modification rates is significant even though the P_o values in the two conditions are both close to unity.

modification rate remains roughly the same. Fig. 9 B shows the averaged results of MTSET modification at three voltages; the modification rates are all the same. On the other hand, the MTSES modification rate of the Y512C mutant varies according to voltages (Fig. 9 C), and the modification shows a consistent pattern—the more depolarized the membrane potential, the slower the MTSES modification rate. This appears to be a state-dependent modification because the change in the modification rate correlates more with the P_o of the channel but not with the membrane voltage. This state-dependent modification is further supported by an experiment in which the MTS modification was conducted in a different $[Cl^-]_o$. In the presence of a higher $[Cl^-]_o$, the fast-gate P_o is larger, and the MTSES modification rate is consistently smaller than that at a low Cl^-, even though the modification voltage is the same (Fig. 9 D). Such a pattern of modification rate is not consistent with a gated access of MTS reagents to the position behind a gate. Instead, it may suggest a gating-associated change in the pore that alters the MTSES modification rate.

DISCUSSION

The present study employs SCAM with charged MTS reagents to examine the accessibility of the amino acid residues of ClC-0 that correspond to those on the helix R of the bacterial ClC channels. The modification pattern from residue 512 to 526 reveals that the modification rate is faster in every third position for both MTSES and MTSET modifications. The most rapid MTSES and MTSET modification rates at four positions (D513C, I516C, K519C, and P522C) are close to the rates of modifying β-ME in the bulk solution, suggesting that these residues are likely to be freely accessible to the applied MTS reagents. These four positions as well as two other positions (I515C and Y523C) that show higher modification rates than those of S123C and Y512C are located on one side of the R helix that faces the permeant ions (Fig. 4 B). These results argue that the structure of the helix R in ClC-0 is likely to be similar to that of the bacterial ClC channels. For the rest of the positions in helix R of ClC-0, MTSES and MTSET can still modify the introduced cysteine with a smaller rate. The fact that the modification occurs at most positions may be ascribed to the possibility that the packing of the helix to the channel is not very tight. Consequently, the crevice between helices may allow MTS reagents to gain access to most positions in helix R.

Besides the helical arrangement of the positions from 512 and 526, we have obtained two other pictures regarding the functions of the ClC-0 channel. First, the inner pore region of ClC-0 strongly selects anionic over cationic MTS reagents. Second, we find no evidence of a physical gate internal to the central Cl^--binding site. We discuss below the implications of MTS modification rates in the intrinsic electrostatic potential of the pore and in the gating mechanism of the channel.

Anion to Cation Selection by the Intrinsic Electrostatic Potential in the Pore

The selection of an anionic over a cationic MTS reagent by the pore of ClC-0 is already present even in modifying the cysteine at the superficial positions such as Y523 and P522. The ratios of MTSES and MTSET modification rates are close to 1 at these positions in contrast to a 12-fold difference for these two compounds to react with the thiol group of β-ME in the

bulk solution (for β-ME, $k'_{MTSES}/k'_{MTSET} = 0.08$; see Stauffer and Karlin, 1994). The selection for anionic over cationic MTS reagents thus may explain the deviations of the K519C and D513C modifications from the general trend of increasing the ratio of k_{MTSES}/k_{MTSET} (Fig. 4 C). This selection for anions is even more prominent as the position of the cysteine is deeper (Fig. 4 C). At the deepest positions, S123C and Y512C, MTSES reacts with these two cysteines two- to fourfold faster than MTSET—transforming into an anion to cation ratio ($k_{MTSES}/k_{MTSET}/0.08$) of 20–50 (Cheung and Akabas, 1997).

To evaluate this charge selection more closely, we adopt the analysis method introduced by Karlin and his colleagues (Pascual and Karlin, 1998; Wilson et al., 2000). The analysis reports the intrinsic electrostatic potential in the pore region under the assumption that the two MTS reagents are similar in all respects except charge. Therefore, the ratio of k_{MTSES}/k_{MTSET} should equal the ratio of the reaction rates of these two reagents with β-ME (k'_{MTSES}/k'_{MTSET}) times a factor ρ that is a function of the intrinsic electrostatic potential in the pore (Pascual and Karlin, 1998; Wilson et al., 2000). Thus,

$$\rho = (k_{MTSES}/k_{MTSET})/(k'_{MTSES}/k'_{MTSET}) \quad (1)$$

and

$$\rho = [-(z_{MTSES} - z_{MTSET})(F/RT)\psi], \quad (2)$$

where z_{MTSES} and z_{MTSET} are the charge on MTSES and MTSET, respectively, F, R, and T have their usual meanings, and ψ is the intrinsic electrostatic potential. From Eqs. 1 and 2, we calculate the values of ρ and ψ for the mutants that show higher MTSES and MTSET modification rates than those of S123C and Y512C mutants (Table I). It can be seen that as the cysteine position becomes deeper in the pore, the value of the electrostatic potential ψ becomes more positive, a design of the pore that helps select anions to enter the pore. These intrinsic electrostatic potentials, however, probably do not reflect the potential at the position where the cysteine is introduced, but report the potential several Å away since MTSES and MTSET molecules are probably 6–7 Å in length (Pascual and Karlin, 1998; Wilson et al., 2000). If residues 512–526 of ClC-0 form an α helix, the linear distance between Y512 and K519 should be ~10–11 Å. Taking into account of the side-chain length of the target cysteine, the charge on the MTS molecules is likely at a position close to the side chain of K519 when MTS reagents efficiently modify the cysteine at the selectivity filter. This may explain the largest anion to cation selection for modifying the Y512C mutant than modifying the cysteine at other positions. On the other hand, when MTS reagents are modifying I515C, the charge on the MTS molecules probably are 5 Å away on the intracellular side of K519.

TABLE I

The Calculated Anion/Cation Selection Ratio and the Intrinsic Electrostatic Potential for Various Cysteine Mutants at the Inner Pore Region

Cysteine mutant	$\rho_{-40\,mV}$	ψ
		mV
Y523C	9.28	28.42
P522C	10.69	30.22
K519C*	1.01	0.14
I516C	15.29	34.78
I515C	23.32	40.16
D513C*	8.09	26.67
S123C	19.41	37.82
Y512C	48.02	49.38

This table lists the values of the anion-cationic selection ratio ρ and the intrinsic electrostatic potential ψ reported by the MTS modifications of the indicated cysteine mutants. $V_{MO} = -40$ mV. The values of ρ and ψ were calculated from Eqs. 1 and 2, respectively. As discussed in the text, the value of ψ probably reports the potential sensed by the charge on the MTS reagent, which is ~10 Å away from the listed cysteine position. The symbol "*" indicates a replacement of a charged residue by cysteine, and therefore the intrinsic electrostatic potential of these mutants show a deviation from the general trend.

The 5-Å distance, however, is short enough for the charged residues at the inner pore mouth to exert their electrostatic influences. Again, we use Eqs. 1 and 2 to calculate the intrinsic electrostatic potential of a location reported by MTS modification of I515C (Table II). In this case, an increase in the total positive charge (or a decrease in the negative charge) on E127 and K519 increases the ratio of k_{MTSES}/k_{MTSET} (Fig. 6 B). The calculated intrinsic electrostatic potential indicates that for an increase of a positive charge at E127 and K519, there is an ~20-mV increase in ψ (Table II). Altering the charge at the positions 127 and 519, however, probably also affects the local pH surrounding I515C because these three residues are close to each other. When the overall charge at positions 127 and 519 is made more positive, the percentage of thiolate species on the I515C side chain is likely to increase. This may explain the U-shape pattern in the MTSET modification rate (Fig. 6 B).

Although the thiolate formation on the thiol group of the introduced cysteine could alter the absolute MTS reaction rate, the changes in the modification rate cancel out by taking the ratio of k_{MTSES}/k_{MTSET}. Therefore, the ratio k_{MTSES}/k_{MTSET} is monotonically increased when the sum of the charges at these two positions is more positive (Fig. 6 B). The roughly staircase jump in the intrinsic electrostatic potential upon altering one total charge at these two positions (~20 mV per charge) suggests that the contributions from these two charges in selecting charged MTS reagents are

TABLE II

The Anion/Cation Selection Ratio and the Intrinsic Electrostatic Potential Reported by MTS Modifications of I515C Mutant

Background	$\rho_{-40\ mV}$	ψ
		mV
Q127/K519 (+1)	82.22	56.24
Q127/M519 (0)	22.57	39.75
E127/K519 (0)	23.32	40.16
Q127/E519 (−1)	6.27	23.41
E127/M519 (−1)	3.45	15.78
E127/E519 (−2)	0.70	−4.54

This table reports the calculated value of ρ and ψ when the reporter cysteine is at position 515 (I515C). $V_{MO} = -40$ mV. The sum of the charges at position 127 and 519 is listed to the right of each 127/519 charge combination. There appears to be a ~20 mV jump in ψ in response to the removal of a negative charge (or the addition of a positive charge).

roughly equal to each other. This is somewhat surprising because E127 has a dominant role in controlling the pore conductance (Chen and Chen, 2003). The difference between the electrostatic control of the pore conductance and the selection of charged MTS molecules probably reflects the importance of the exact positions of the interacting charges. In the case of conductance regulation, the fixed internal Cl^--binding sites are closer to E127 than to K519 (Dutzler et al., 2003). However, for MTS modification of I515C, since MTS molecules are long, the charge on the MTS compounds is probably moving randomly outside the internal pore entrance. The selection of the charged MTS reagent therefore may come from the averaged contributions from these two residues.

Implication of MTS Modification Rate on the Gating Mechanism

ClC-0 has been known to have two different gating mechanisms—the fast and the slow (inactivation) gating. Which gating mechanism corresponds to the operation of the E166 side chain? By comparing the MTS modification rate at different conditions, we found that the accessibility to MTS compounds in all positions from the pore mouth to the Cl^- selectivity filter is not higher when the channel is in the open state. Therefore, a physical gate like the one proposed in voltage-gated Shaker K^+ channel (Liu et al., 1997) to gate the access of MTS reagents to the pore is unlikely to be located at a position internal to the selectivity filter. However, there appears to be a very peculiar state-dependent modification that is very obvious in the MTSES modification of the Y512C mutant. This apparent state-dependence is in direct opposition to that observed in the Shaker K^+ channel—the modification rate is faster when the gate is closed. The effect is not due to a voltage dependence of MTS modification because the MTSES modification rate can be reduced at the same voltage if the P_o is elevated through raising $[Cl^-]_o$ (Fig. 9 D).

The apparent state dependence of Y512C is interesting in that the phenomenon is observed only when MTSES is used as the modifying reagent. Several possibilities might explain this phenomenon, yet each one having its own weakness. First, it might be possible that the side chain of Y512 is part of the fast gate, and when the gate is closed, this side chain directly points to the pore, and thus is more accessible to the MTS reagents in the pore. This proposal faces a severe problem because a similar state dependence would have occurred for MTSET modification. A second possibility is that perhaps in the open state, Cl^- ions coming from the extracellular side would physically knock off the MTS molecule in the pore, thus reduce the probability for the molecule to react with the cysteine at the selectivity filter. This argument is also weak because only Y512C mutant has such a state-dependent effect while the cysteine at other pore positions, such as S123C, does not show this phenomenon. In addition, if this were the mechanism, one should have observed at least part of the knock-off effect for the MTSET modification even though the interaction of Cl^- with MTSES and MTSET might not be exactly the same. The third possibility is that perhaps the fast gate is right behind Y512C (for example, the side chain of E166), and when the gate is open, the MTS reagent is pushed through the pore. Thus, MTS reagents can stay at the selectivity filter longer to react with Y512C when the gate is closed than when the gate is open. This argument again is not strong. Besides the same problem that a similar state-dependent modification does not occur for the S123C mutant, it is not known if a large molecule like MTSES can punch through the pore of ClC-0. The above proposals thus do not reasonably explain this peculiar state-dependent MTSES modification.

In the literature of MTS modification studies, a similar MTSES-only, state-dependent modification was observed when MTS modifications were used to evaluate the proximity of the outer end of the S4 segment to an external pore residue in Shaker K^+ channel (Elinder et al., 2001). It was proposed that an increase in the local electrostatic potential due to the appearance of a positive charge can have two effects: the attraction or repulsion of MTS reagents to the reporter cysteine and an increase of the deprotonated state (the thiolate) of the thiol group of the reporter cysteine. These two effects which arise from an approaching positive charge (increase MTSES concentration and thiolate formation) both lead to a higher rate of MTSES modification, but they cancel out each other in the MTSET modification. In ClC-0, the electrostatic potential in the pore is prominent as judged from its controls in the ion flux (Chen

and Chen, 2003) and in the selection of different charged MTS reagents (the above results). If during the fast-gate opening process a negative charge comes into the pore (or a positive charge moves away from the pore), the reduction in the electrostatic potential will reduce the MTSES modification rate. What are the potential sources for the change of the electrostatic potential in the pore? There are charged residues in the pore of ClC-0, including the side chain of E166 that may serve as the gate. The protein conformational change in the fast gating process surely involves a rearrangement of the positions of these charged residues, and this could result in a different intrinsic electrostatic potential between the closed and the open channels. Another possibility that could result in the changes in the intrinsic electrostatic potential comes from the binding of Cl^- to the pore when the channel is open. This possibility is directly suggested by the result in Fig. 9 D, in which the MTSES modification rates of the fully open Y512C pore are not the same when Cl^- concentrations are different. For example, at 60 mV, the fast-gate P_o of Y512C mutant is close to unity at both 4 and 142 mM $[Cl^-]_o$. However, different MTSES modification rates are observed under these two conditions—the higher the $[Cl^-]_o$, the smaller the MTSES modification rate.

In summary, three conclusions emerge from the present study. First, the MTS modification pattern suggests that the overall alignments of the residues on helix R in the inner pore region are quite similar between ClC-0 and the bacterial ClC channels—the hot residues face the permeant ions as if these residues line the wall of the ion permeation pathway (Fig. 4 B). Second, there is no moving structure on the intracellular side of the selectivity filter, which can physically gate the access of intracellular MTS reagents in response to the opening and closing of the fast gate. Thus, the hypothesis of the side chain of E166 being the fast gate of the channel is applicable to ClC-0. Finally, the electrostatic potential of the ClC-0 pore is prominent. This intrinsic potential in the pore is not only important in selecting charged MTS reagents, but is also likely responsible for the apparent state-dependent modification of Y512C. As the electrostatic potentials of ClC-0 pore is also critical for the functional properties of the channel, understanding the state-dependent MTSES modification on Y512C mutant may help further explore the gating and permeation of ClC-0.

We are grateful to Dr. R. Fairclough and Dr. T.-C. Hwang for the helpful discussions in the process of the work and for the critical readings of the manuscript.

This work was partly supported by a Health Science Research Award from University of California at Davis School of Medicine and a National Institutes of Health grant GM-65447.

Olaf S. Andersen served as editor.

Submitted: 7 April 2003
Accepted: 7 July 2003

REFERENCES

Akabas, M.H., D.A. Stauffer, M. Xu, and A. Karlin. 1992. Acetylcholine receptor channel structure probed in cysteine-substitution mutants. *Science.* 258:307–310.

Chen, M.-F., and T.-Y. Chen. 2001. Different fast-gate regulation by external Cl^- and H^+ of the muscle-type ClC chloride channel. *J. Gen. Physiol.* 118:23–32.

Chen, M.-F., and T.-Y. Chen. 2003. Side-chain charge effects and conductance determinants in the pore of ClC-0 chloride channel. *J. Gen. Physiol.* 122:133–145.

Chen, T.-Y. 1998. Extracellular zinc ion inhibits ClC-0 chloride channels by facilitating slow gating. *J. Gen. Physiol.* 112:715–726.

Chen, T.-Y., and C. Miller. 1996. Nonequilibrium gating and voltage dependence of the ClC-0 Cl^- channel. *J. Gen. Physiol.* 108:237–250.

Cheung, M., and M.H. Akabas. 1997. Locating the anion-selectivity filter of the cystic fibrosis transmembrane conductance regulator (CFTR) chloride channel. *J. Gen. Physiol.* 109:289–299.

Doyle, D.A., J. Morais Cabral, R.A. Pfuetzner, A. Kuo, J.M. Gulbis, S.L. Cohen, B.T. Chait, and R. MacKinnon. 1998. The structure of the potassium channel: Molecular basis of K^+ conduction and selectivity. *Science.* 280:69–77.

Dutzler, R., E.B. Campbell, M. Cadene, B.T. Chait, and R. MacKinnon. 2002. X-ray structure of a ClC chloride channel at 3.0 Å reveals the molecular basis of anion selectivity. *Nature.* 415:287–294.

Dutzler, R., E.B. Campbell, and R. MacKinnon. 2003. Gating the selectivity filter in ClC chloride channels. *Science.* 300:108–112.

Elinder, F., R. Mannikko, and H.P. Larsson. 2001. S4 charges move close to residues in the pore domain during activation in a K channel. *J. Gen. Physiol.* 118:1–10.

Fahlke, Ch., H.T. Yu, C.L. Beck, T.H. Rhodes, and A.L. George, Jr. 1997. Pore-forming segments in voltage-gated chloride channels. *Nature.* 390:529–532.

Hanke, W., and C. Miller. 1983. Single chloride channels from *Torpedo* electroplax: activation by protons. *J. Gen. Physiol.* 82:25–45.

Hamill, O.P., A. Marty, E. Neher, B. Sakmann, and F.J. Sigworth. 1981. Improved patch-clamp techniques for high-resolution current recording from cells and cell-free membrane patches. *Pflugers Arch.* 391:85–100.

Hille, B. 2001. Potassium channels and chloride channels. *In* Ion Channel of Excitable Membrane. 3rd ed. B. Hille, editor. Sinauer Associates, Inc., Sunderland, MA. 131–167.

Jentsch, T.J., T. Friedrich, A. Schriever, and H. Yamada. 1999. The CLC chloride channel family. *Pflügers Arch.-Eur. J. Physiol.* 437: 783–795.

Jentsch, T.J., V. Stein, F. Weinreich, and A. Zdebik. 2002. Molecular structure and physiological function of chloride channels. *Physiol. Rev.* 82:503–568.

Jentsch, T.J., K. Steinmeyer, and G. Schwarz. 1990. Primary structure of *Torpedo marmorata* chloride channel isolated by expression cloning in *Xenopus* oocytes. *Nature.* 348:510–514.

Karlin, A., and M.H. Akabas. 1998. Substituted-cysteine-accessibility method. *In* Methods in Enzymology. Vol. 293. P.M. Conn, editor. Academic Press Inc., San Diego, CA. 123–136.

Lin, Y.-W., C.-W. Lin, and T.-Y. Chen. 1999. Elimination of the slow gating of ClC-0 chloride channel by a point mutation. *J. Gen. Physiol.* 114:1–12.

Lin, C.-W., and T.-Y. Chen. 2000. Cysteine modification of a putative pore residue in ClC-0: implication for the pore stoichiometry of ClC chloride channels. *J. Gen. Physiol.* 116:535–546.

Liu, Y., M. Holmgren, M.E. Jurman, and G. Yellen. 1997. Gated ac-

cess to the pore of a voltage-dependent K^+ channel. *Neuron.* 19: 175–184.

Lu, T., Y.-G. Zhu, and J. Yang. 1999. Cytoplasmic amino and carboxyl domains form a wide intracellular vestibule in an inwardly rectifying potassium channel. *Proc. Natl. Acad. Sci. USA.* 96:9926–9931.

Lu, Q., and C. Miller. 1995. Silver as a probe of pore-forming residues in a potassium channel. *Science.* 268:304–307.

Ludewig, U., T.J. Jentsch, and M. Pusch. 1997. Analysis of a protein region involved in permeation and gating of the voltage-gated *Torpedo* chloride channel ClC-0. *J. Physiol.* 498:691–702.

Ludewig, U., M. Pusch, and T.J. Jentsch. 1996. Two physically distinct pores in the dimeric ClC-0 chloride channel. *Nature.* 383: 340–343.

Maduke, M., C. Miller, and J.A. Mindell. 2000. A decade of CLC chloride channels: structure, mechanism, and many unsettled questions. *Annu. Rev. Biophys. Biomol. Struct.* 29:411–438.

Middleton, R.E., D.J. Pheasant, and C. Miller. 1994. Purification, reconstitution, and subunit composition of a voltage-gated chloride channel from *Torpedo* electroplax. *Biochemistry.* 33:13189–13198.

Middleton, R.E., D.J. Pheasant, and C. Miller. 1996. Homodimeric architecture of a ClC-type chloride ion channel. *Nature.* 383:337–340.

Miller, C. 1982. Open-state substructure of single chloride channels from *Torpedo electroplax. Phil. Trans. R. Soc. Lond. B. Biol. Sci.* 299: 401–411.

Miller, C., and E.A. Richard. 1990. The *Torpedo* chloride channel: intimations of molecular structure from quirks of single-channel function. *In* Chloride Transporters. A. Leefmans and J. Russel, editors. Plenum Press, New York. 383–405.

Miller, C., and M.M. White. 1984. Dimeric structure of single chloride channels from *Torpedo* electroplax. *Proc. Natl. Acad. Sci. USA.* 81:2772–2775.

O'Neill, G.P., R. Grygorczyk, M. Adam, and A.W. Ford-Hutchinson. 1991. The nucleotide sequence of a voltage-gated chloride channel from the electric organ of *Torpedo californica. Biochim. Biophys. Acta.* 1129:131–134.

Pascual, M.J., and A. Karlin. 1998. State-dependent accessibility and electrostatic potential in the channel of acetylcholine receptor: Inferences from rates of reaction of thiosulfonate with substituted cysteines in the M2 segment of the α subunit. *J. Gen. Physiol.* 111:717–739.

Pusch, M., U. Ludewig, A. Rehfeldt, and T.J. Jentsch. 1995. Gating of the voltage-dependent chloride channel ClC-0 by the permeant anion. *Nature.* 373:527–531.

Reeves, D.C., E.N. Goren, M.H. Akabas, and S.C.R. Lummis. 2001. Structural and electrostatic properties of the 5-HT_3 receptor pore revealed by substituted cysteine accessibility mutagenesis. *J. Biol. Chem.* 276:42035–42042.

Stauffer, D.A., and A. Karlin. 1994. Electrostatic potential of the acetylcholine binding sites in the nicotinic receptor probed by reactions of binding-site cysteines with charged methanethiosulfonates. *Biochemistry.* 33:6840–6849.

Wilson, G.G., J.M. Pascual, N. Brooijmans, D. Murray, and A. Karlin. 2000. The intrinsic electrostatic potential and the intermediate ring of charge in the acetylcholine receptor channel. *J. Gen. Physiol.* 115:93–106.